IGS

Author for correspondence:
William D. Harcourt;
Email: william.harcourt@abdn.ac.uk

cambridge.org/aog

Glacier monitoring using real-aperture 94 GHz radar

William D. Harcourt[1,2] iD, Duncan A. Robertson[1] iD, David G. Macfarlane[1] iD, Brice R. Rea[2] iD, Matteo Spagnolo[2] iD, Douglas I. Benn[3] iD and Mike R. James[4] iD

[1]SUPA School of Physics and Astronomy, University of St Andrews, St Andrews, UK; [2]School of Geosciences, University of Aberdeen, Aberdeen, UK; [3]School of Geography & Sustainable Development, University of St Andrews, St Andrews, UK and [4]Lancaster Environment Centre, Lancaster University, Lancaster, UK

Abstract

Close-range sensors are employed to observe glaciological processes that operate over short timescales (e.g. iceberg calving, glacial lake outburst floods, diurnal surface melting). However, under poor weather conditions optical instruments fail while the operation of radar systems below 17 GHz do not have sufficient angular resolution to map glacier surfaces in detail. This letter reviews the potential of millimetre-wave radar at 94 GHz to obtain high-resolution 3-D measurements of glaciers under most weather conditions. We discuss the theory of 94 GHz radar for glaciology studies, demonstrate its potential to map a glacier calving front and summarise future research priorities.

Introduction

Close-range sensors are defined as systems which are deployed up to ∼20 km from a glacier and collect remote-sensing measurements at high spatio-temporal resolution. They are commonly used to monitor glaciological processes that operate over timescales of minutes to days and over spatial scales of metres to kilometres. This is particularly important for measuring mass loss processes such as iceberg calving and surface ablation (Fischer and others, 2016; How and others, 2019; Xie and others, 2019) in order to quantify glacier mass balance. It is also critical for rapid monitoring of glacier hazards such as glacial lake outburst floods (Taylor and others, 2021) which can lead to significant infrastructure damage and loss of life. In contrast to airborne and spaceborne systems, close-range ground-based sensors are capable of monitoring glaciers from a range of viewing geometries. A combination of electro-optical sensors (e.g. time-lapse cameras, digital cameras onboard uncrewed air vehicles, terrestrial laser scanners (TLSs)) and low (L- to C-bands) to medium (X- to Ku-bands) resolution ground-based radars have been used to monitor glaciers at close range. Electro-optical sensors can acquire detailed measurements but their performance degrades under conditions of reduced visibility. Low-to-medium resolution radar systems can obtain measurements under adverse weather conditions but the angular resolution of their measurement is coarse (Fig. 1). The potential of real-aperture millimetre-wave radars at 94 GHz, which offers a compromise in resolution and penetration through obscuring conditions, as a new tool for glacier monitoring is explored below.
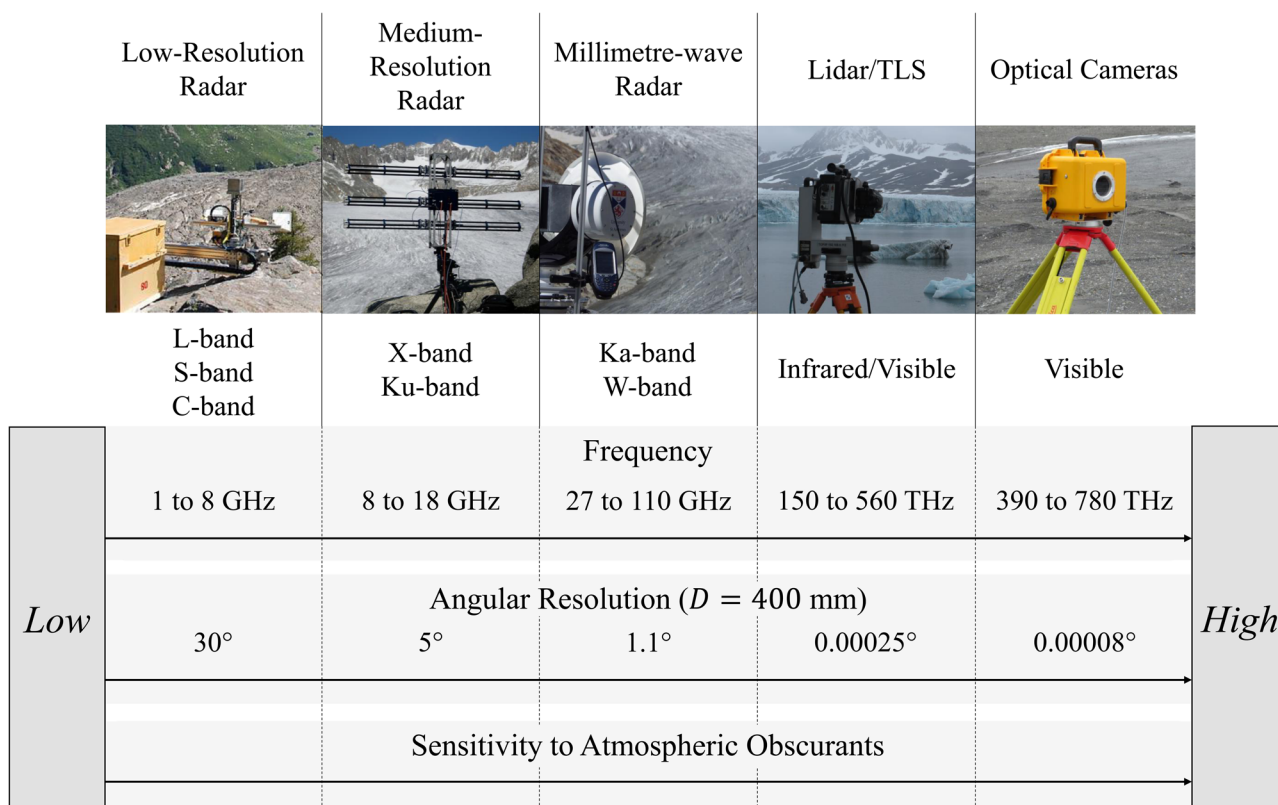
94 GHz radar for glacier monitoring

Millimetre-wave radars operate in the frequency range of 30–300 GHz (wavelengths of 1 mm to 1 cm) (Currie and Brown, 1987), although most remote-sensing studies are carried out in the low absorption 'atmospheric windows' near 35 GHz (Ka-band) and 94 GHz (W-band). While a handful of studies have mapped glacier and snow surfaces between 27 and 40 GHz (Ka-band) (Sadowy and others, 2007; Moller and others, 2011), there are no studies that have used 94 GHz (W-band) for this purpose despite the potential advantages of using higher frequency radar systems for close-range sensing of cryospheric terrain.

The measurement capabilities of a close-range sensor depends on its angular (θ_r) and range (ΔR) resolution. The angular resolution of an imaging sensor increases linearly with operating wavelength (λ):

$$\theta_r = 1.22 \frac{\lambda}{D} \tag{1}$$

where D is the size of the aperture (e.g. a lens, an antenna). The angular resolution of conventional terrain mapping radar systems operating between 1 and 18 GHz (i.e. L-band to Ku-band) is lower than electro-optical systems such as TLS and digital cameras due to the longer wavelength of lower frequency radars. However, electro-optical surveying techniques operating in the visible/infrared range become significantly attenuated when obscurants (e.g. rain, fog, dust) are present in the atmosphere (Fig. 1). Operating at higher radar frequencies such as 94 GHz increases the sensor angular resolution (i.e. higher value of λ) and permits the use of real-beam scanning for mapping glacier topography. In comparison, extracting

Low-Resolution Radar	Medium-Resolution Radar	Millimetre-wave Radar	Lidar/TLS	Optical Cameras
L-band S-band C-band	X-band Ku-band	Ka-band W-band	Infrared/Visible	Visible

	Frequency					
Low	1 to 8 GHz	8 to 18 GHz	27 to 110 GHz	150 to 560 THz	390 to 780 THz	*High*
	Angular Resolution ($D = 400$ mm)					
	30°	5°	1.1°	0.00025°	0.00008°	
	Sensitivity to Atmospheric Obscurants					

Figure 1. Close-range sensing continuum illustrating the trade-off between sensor operating frequency, angular resolution (calculated from Eqn (1), where λ is taken to be the centre wavelength of the defined frequency range and D is set constant at 400 mm), and sensitivity to atmospheric obscurants. Lower frequency radar systems are sub-divided into 'low-resolution radar' (1–8 GHz) and 'medium-resolution radar' (8–18 GHz). Low-resolution radar image is taken from Noferini and others (2009) and medium-resolution radar image is taken from Werner and others (2008).

topographical datasets from phase-based interferometric systems is complicated by temporal decorrelation between scans, which significantly reduces the accuracy of 3-D measurements (Werner and others, 2008; Xie and others, 2019). The finer angular resolution for a given antenna diameter (D) at 94 GHz also increases antenna gain (Stutzman, 1998) which improves radar signal-to-noise ratio (SNR) and enables the use of lower transmit powers which is advantageous for low power use in field deployment.

On the contrary, range resolution mostly relates to active sensors (e.g. radar, TLS) and is defined by:

$$\Delta R = \frac{c}{2B} \qquad (2)$$

where c is the speed of light (3×10^8 m s^{-1}) and B is the frequency bandwidth over which the system operates. Millimetre-wave radar systems can achieve high range resolution using wide frequency bandwidths because they are only modest fractional bandwidths (i.e. B/f_c where f_c is the sensor operating frequency) and are technologically easier to achieve. This is beneficial when mapping environments with steep slopes such as glacier calving fronts where a high range resolution is required for tracking changes in the range direction.

The short wavelength of 94 GHz radar (3.19 mm) is also of the same magnitude as the typical size of ice crystals on glacier surfaces (i.e. millimetres to centimetres) hence scattering is mostly diffuse. This increases the probability of radar backscatter when the radar beam is almost perpendicular to the local surface normal (incidence angles above 70°) which enables 94 GHz radar to map glacier surfaces at a wide range of viewing angles. 94 GHz radar backscatter is therefore also more sensitive to glacier

surface changes than lower frequency radars, which could be used to assess patterns of surface melt and snow accumulation over time. Finally, signal penetration into ice is negligible at 94 GHz (Petrenko and Whitworth, 2006; Hensley and others, 2016) which removes the need for surface corrections in repeat 3-D measurements.

Altogether, the principal benefit of using millimetre-wave radars for terrain mapping is its ability to acquire high angular resolution measurements for a given aperture size under conditions of reduced visibility using compact systems (i.e. small value of D) (Currie and Brown, 1987), which is important for close-range sensors that are deployed in the field. This cannot be achieved using electro-optical sensors or lower frequency radar systems (Fig. 1), lending support for this technique in the remote sensing of glaciers.

Theoretical performance

To demonstrate the low sensitivity of 94 GHz radar to atmospheric obscurants, we simulated the impact of four weather conditions (clear atmosphere, fog, rain and falling snow) on the SNR of the real-aperture, 2nd generation All-weather Volcano Topography Imaging Sensor (AVTIS2) 94 GHz frequency-modulated continuous wave radar developed at the University of St Andrews (full details in Macfarlane and others, 2013). SNR was calculated as a function of range (R) using:

$$SNR = \frac{P_r(R)}{N_0(R)} \qquad (3)$$

where P_r is the radar received power and N_0 is the radar noise floor. We used the radar range equation in the range-bin limited

case (Macfarlane and others, 2013; Ulaby and others, 2019) alongside atmospheric attenuation models in Matlab (Gunn and East, 1954; ITU-R, 2005, 2013a, 2013b) to predict P_r. The variation of the AVTIS2 noise floor power level (N_0) with range has been previously characterised (Section 3.4.3 in Harcourt, 2022) and is 10–20 dB higher between 0 and 2.3 km compared to 2.3 and 6 km. This leads to the non-linear radar curves shown in Figure 2, noting that the increase between 2 and 2.5 km results from the reduction in the noise floor power level at these ranges (frequencies) (Eqn (3)).

AVTIS2 performs well in both good and poor visibility with little atmospheric attenuation (Fig. 2a). Attenuation when operating AVTIS2 under clear weather conditions reaches 0.46 dB km^{-1} which leads to a maximum SNR of ~24 dB at 6 km for terrain with a reflectivity (σ^0) of −10 dB. Increases in atmospheric attenuation are primarily due to atmospheric water vapour density which may be large near water bodies such as the ocean which is pertinent for deployment of 94 GHz radar systems in locations such as glacier calving fronts. In dense fog where the liquid water density is 0.5 g m^{-3}, atmospheric attenuation is 2 dB km^{-1} which is significant for long-range performance as this reduces the SNR for terrain with a σ^0 of −10 dB to below 10 dB. For terrain with lower values of σ^0, dense fog may reduce the target detectability to within 4 km. In general, Figure 2a demonstrates that AVTIS2 is expected to perform well under both clear weather and many reduced visibility conditions.

The impact of rain and snow precipitation on 94 GHz radar performance is much greater (Fig. 2b). The greatest impact is under conditions of heavy rain (10 mm h^{-1}), where the radar model predicts high attenuation (9.4 dB km^{-1}). Under such conditions, AVTIS2 cannot measure terrain backscatter beyond 3.5 km and, given the shape of the noise floor, backscatter beyond 2 km is likely to be weak. For terrain with a smaller value of σ^0, the maximum detectable range will reduce and degrade radar performance considerably. The radar performance in light rain (1

mm h^{-1}) remains suitable for long-range mapping with a possible SNR of ~17 dB at 6 km for terrain with a σ^0 of −10 dB. In comparison, the impact of snowfall on atmospheric attenuation is smaller. Heavy snow has a similar attenuation rate to dense fog (2 dB km^{-1}) and hence long-range mapping is possible under such conditions. Both rain and snow are common in mountainous and high latitude regions where glaciers and ice sheets are found, hence the predicted performance demonstrates the suitability of AVTIS2 for monitoring glaciers.

## From 2-D to 3-D observations

A case study of mapping the Hansbreen calving front in Svalbard (Fig. 3a; Harcourt and others, 2022) is used here to illustrate the 2-D and 3-D datasets that 94 GHz radar can generate. Hansbreen terminates at sea level across a ~1.5 km wide calving front. AVTIS2 was deployed to the west of the Hansbreen terminus, where the distance to the calving front ranged between 0.5 and 1.5 km. There were no clouds or precipitation at the time of data collection, hence atmospheric attenuation was low and primarily due to gases (Fig. 2). AVTIS2 transmits a sawtooth chirp pattern along each Line of Sight (LoS) with a transmit power of 16.35 dBm and acquires 3-D data cubes of radar backscatter at each range bin, azimuth angle and elevation angle. AVTIS2 scanned an angular area 83° × 5° in azimuth and elevation, respectively. The angular increment was 0.045° in azimuth and 0.2° in elevation and the scan time for this angular set up was ~30 min. By calculating the maximum radar received power at each range bin within the 3-D data cube, 2-D SNR images can be created and an example from a scan of the Hansbreen tidewater glacier in Svalbard is shown in Figure 3b.

The calving front can be distinguished by SNR values above 20 dB compared to the open water that has SNR values below 8 dB. The width of the calving front was estimated to be 10–15 m at 1 km and 30–35 m at 1.5 km. This difference is due to: (1) the increase in the radar spot size with range (6 m km^{-1}), (2) the variable geometry of the ice cliff and (3) the effect of combining scans at different elevations (i.e. different levels of the data cube). Theoretically, the minimum mapping resolution is determined by the range resolution which was set to 0.38 m in this study. Icebergs that range in size from 40 to 480 m^2 can be observed in front of the ice terminus along with ocean waves that manifest as streaks of low SNR values (8–12 dB) surrounding the icebergs. The complex pattern of crevasses behind the calving front can also be clearly observed, the smallest of which were 3 m wide. When collected in a time series, these images could be used for estimating ice velocity using speckle tracking, mapping the position of the calving front and assessing ice surface characteristics over time based on changes in SNR.

3-D point clouds of glacier calving fronts can also be generated by calculating the range to maximum SNR along each LoS at each azimuth and elevation angle scanned by the radar. An example is shown in Figure 3c. The calving front contains both vertical ice cliffs that range between 30 and 50 m in height as well as 3-D structures that extend across a calving zone. The vertical resolution of the 3-D data was ~4 m at 1 km and ~6 m at 1.5 km. This can be reduced by minimising the vertical sampling interval to 0.05° but this increases scan times. Therefore, future deployments of the AVTIS2 radar should ensure that the viewing geometry maximises measurement of changes in the radar range direction e.g. parallel to ice flow to measure glacier velocity. The 3-D point cloud also includes crevasses immediately upstream of the terminus and icebergs in the fjord. Gaps in the point cloud exist where the radar beam is obstructed by the ice cliff. This point cloud was derived without interferometry and, critically, can be acquired under most weather conditions, as shown
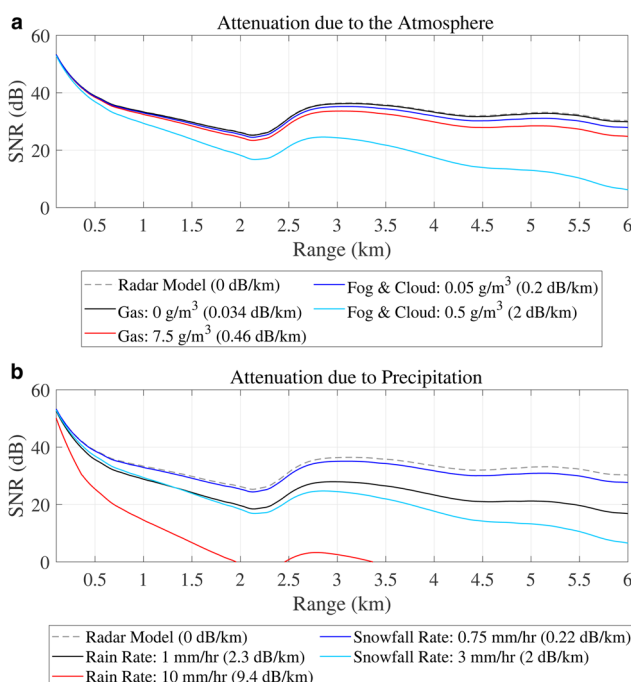
Figure 2. Predicted radar performance in terms of SNR using the radar range equation with a terrain reflectivity (σ^0) of −10 dB. (a) Attenuation due to atmospheric gases (primarily caused by absorption due to oxygen and water vapour) and fog, both modelled with a 15° air temperature, while gas attenuation was modelled under the additional constraint of an atmospheric pressure of 101.3 kPa. (b) Attenuation due to light/heavy rainfall and snowfall.
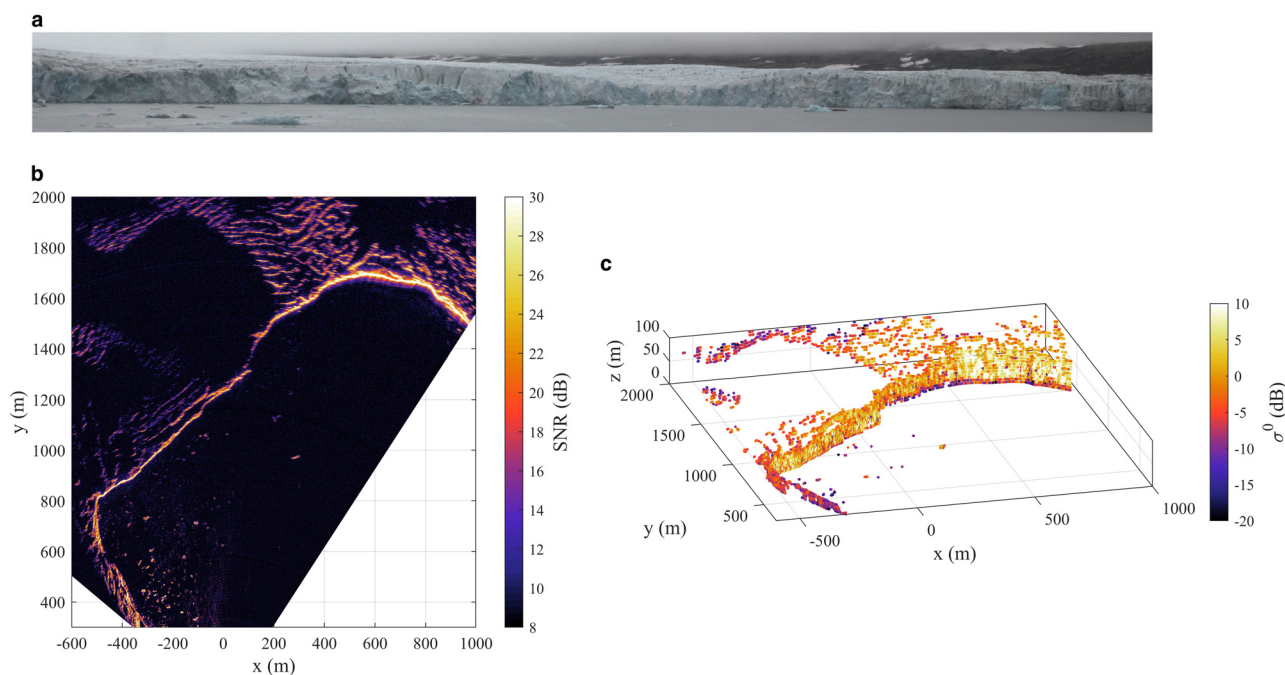
Figure 3. (a) Time-lapse image of the Hansbreen calving front, (b) 2-D image of the Hansbreen terminus captured using AVTIS2 and (c) a 3-D point cloud of the Hansbreen calving front derived from AVTIS2 94 GHz radar data.

in the previous section. Therefore, 94 GHz radar systems such as AVTIS2 can be used to record near-continuous records of 3-D ice front change when deployed at close ranges of a few kilometres.

Future development

Future development of 94 GHz radar for glacier monitoring should prioritise four key areas:

(1) *Assessment of capabilities to monitor glaciers of different dynamics and sizes*: Future studies should investigate the capabilities of monitoring iceberg calving at larger and more dynamic tidewater glaciers such as outlets from the Greenland ice sheet, in particular the impact on data acquisition rates, spatial coverage and data correction due to glacier movement within scans. 94 GHz radar could be used for continuous monitoring of hanging glaciers in mountain regions in order to detect changes in ice dynamics that may represent a precursor to glacier collapse. This will enable an understanding of its potential as a hazard warning system to complement existing interferometric and Doppler radar systems (Margreth and others, 2017). Understanding optimum radar viewing geometries should also be assessed in order to characterise radar performance. This is critical to understand limitations of different field locations for future radar deployments. These future applications all currently require radar systems such as AVTIS2 to be positioned on stable ground. If the x, y and z positions of the radar system could be tracked accurately over time using an inertial measurement unit or GPS, a 94 GHz radar system could in theory be deployed on a glacier to map e.g. supraglacial lakes on the surface of an ice sheet, or crevasse propagation.

(2) *Collection of radar backscatter measurements from a range of ice surface types*: A statistically significant database of 94 GHz radar backscatter data from a variety of ice surface conditions in different viewing geometries should be generated to improve both radar performance prediction and the characterisation of ice surface conditions. For example, collecting radar backscatter measurements across glacier surfaces over a diurnal melt and refreezing cycle will enable a better understanding of how surface meltwater impacts radar backscatter, hence improving the interpretation of radar backscatter time series. Additional measurements should also be sought from glacier calving fronts, alpine glacier ice (refrozen and melting), firn, 'cold' ice, and 'warm' ice to identify whether such surfaces can be distinguished within 94 GHz radar backscatter data. Measurements from different topographic features, such as seracs, crevasses (of different size and density), supraglacial streams, supraglacial lakes and moulins will also improve understanding of how such features impact radar backscatter. Together, this may enable the implementation of new techniques, such as machine learning, to classify ice surfaces from 94 GHz radar data for improved glacier surface characterisation.

(3) *Improve real-aperture 94 GHz radar processing workflows*: More accurate retrievals of surface elevation from AVTIS2 3-D data cubes and improved radar calibration for quantifying radar reflectivity (σ^0) will be critical for realising the full potential of 94 GHz radar for glacier studies. For example, extracting more points in a 3-D point cloud by analysing the full backscattered waveform of 94 GHz radars will enable more detailed multi-temporal point cloud comparisons and hence a better understanding of glacier processes. Further, 2-D azimuth-elevation maps of radar backscatter are often dominated by large scattering objects that spread across the scene due to the two-way convolution of the antenna pattern. Deconvolution filters could be used to remove these effects. Signal attenuation due to rain is partly caused by scattering from water droplets and this can be significant in heavy rainfall, leading to more radar backscatter. This can lead to false alarms and the extraction of anomalous points, hence developing signal processing techniques to remove these points is crucial for improving the performance of surface extraction techniques and automating the process.

(4) *Improvement in the practical deployment of 94 GHz radar systems in the field*: Future research should include better

performance characterisation, improved calibration procedures and automated georeferencing routines. Firstly, the temperature sensitivity of radar systems such as AVTIS2 should be characterised (e.g. using cold chambers) in order to understand its influence on radar hardware and therefore radar performance. Secondly, methods to convert radar received power to normalised radar cross section without calibration targets (e.g. trihedral corner reflectors) should be developed in order to maximise glacier scan times and improve the temporal resolution of radar measurements. A combination of atmospheric attenuation modelling and using spatially variable radar propagation factors over heterogeneous surface types could be used here but this would require extensive testing to ensure its reliability. Recording meteorological data concurrently, for example a local meteorological station, would also enable accurate weather measurements to be used for this analysis. Lastly, using the technique of direct georeferencing to geolocate AVTIS2 point clouds would remove the need to deploy ground control points in the field (Jaud and others, 2013; Hartzell and others, 2015) and also maximises scan times which will improve the temporal resolution of measurements.

Summary

The unique capabilities of millimetre-wave radars used at 94 GHz to obtain high angular resolution measurements of glacier surfaces under conditions of reduced visibility have been demonstrated. In particular, the dual acquisition of high-resolution 2-D radar images and 3-D point clouds under most weather conditions is a significant improvement upon previous close-range sensors that have been used to monitor glaciers. This is critical for improving our understanding of processes such as iceberg calving, glacial lake outburst floods and diurnal melting and refreezing cycles. Using the suggested future research priorities, 94 GHz radar can be realised as a unique tool for glaciology and cryospheric sciences in general.

References

Currie NC and Brown CE (1987) *Principles and Applications of Millimetre Wave Radar*. Norwood, MA: Artech House.

Fischer M, Huss M, Kummert M and Hoelzle M (2016) Application and validation of long-range terrestrial laser scanning to monitor the mass balance of very small glaciers in the Swiss Alps. *The Cryosphere* **10**(3), 1279–1295.

Gunn KL and East TW (1954) The microwave properties of precipitation particles. *Quarterly Journal of the Royal Meteorological Society* **80**, 522–545.

Harcourt WD (2022) *The application of millimetre-wave radar to the study of the cryosphere*. Ph.D. thesis. University of St Andrews.

Harcourt WD and 9 others (2022) Millimetre-wave radar observations of glacier calving at Hansbreen (Svalbard) correlated with TLS, time-lapse camera images and seismic records. In *EGU General Assembly*, Vienna, Austria.

Hartzell PJ, Gadomski PJ, Glennie CL, Finnegan DC and Deems JS (2015) Rigorous error propagation for terrestrial laser scanning with application to snow volume uncertainty. *Journal of Glaciology* **61**(230), 1147–1158.

Hensley S, Moller D, Oveisgharan S, Michel T and Wu X (2016) Ka-band mapping and measurements of interferometric penetration of the Greenland ice sheets by the GLISTIN radar. *IEEE Journal of Selected Topics in Applied Earth Observations and Remote Sensing* **9**(6), 2436–2450.

How P and 8 others (2019) Calving controlled by melt-under-cutting: detailed calving styles revealed through time-lapse observations. *Annals of Glaciology* **60**(78), 20–31.

ITU-R (2005) Recommendation ITU-R p.838-3: Specific attenuation model for rain.

ITU-R (2013a) Recommendation ITU-R p.676-10: Attenuation by atmospheric gases.

ITU-R (2013b) Recommendation ITU-R p.840-6: Attenuation due to clouds and fog.

Jaud M, Rouveure R, Faure P and Monod MO (2013) Methods for FMCW radar map georeferencing. *ISPRS Journal of Photogrammetry and Remote Sensing* **84**, 33–42.

Macfarlane DG and 5 others (2013) Topographic and thermal mapping of volcanic terrain using the AVTIS ground-based 94-GHz dual-mode radar/radiometric imager. *IEEE Transactions on Geoscience and Remote Sensing* **51**(1), 455–472.

Margreth S and 5 others (2017) Analysis of the hazard caused by ice avalanches from the hanging glacier on the Eiger West face. *Cold Regions Science and Technology* **144**, 63–72.

Moller D and 6 others (2011) The glacier and land ice surface topography interferometer: an airborne proof-of-concept demonstration of high-precision Ka-band single-pass elevation mapping. *IEEE Transactions on Geoscience and Remote Sensing* **49**(2), 827–842.

Noferini L, Mecatti D, Macaluso G, Pieraccini M and Atzeni C (2009) Monitoring of Belvedere Glacier using a wide angle GB-SAR interferometer. *Journal of Applied Geophysics* **68**(2), 289–293.

Petrenko VF and Whitworth RW (2006) *Physics of Ice*. New York, USA: Oxford University Press.

Sadowy G and 5 others (2007) Technology demonstration of Ka-band digitally-beam formed radar for ice topography mapping. In *2007 IEEE Aerospace Conference*, pp. 1–10, IEEE.

Stutzman WL (1998) Estimating directivity and gain of antennas. *IEEE Antennas and Propagation Magazine* **40**(4), 7–11.

Taylor LS and 5 others (2021) Remote sensing of the mountain cryosphere: current capabilities and future opportunities for research. *Progress in Physical Geography: Earth and Environment* **45**(6), 931–964.

Ulaby F, Dobson MC and Álvarez-Pérez JL (2019) *Handbook of Radar Scattering Statistics for Terrain*. Norwood, MA: Artech House.

Werner C, Strozzi T, Wiesmann A and Wegmuller U (2008) A real-aperture radar for ground-based differential interferometry. In *IGARSS 2008–2008 IEEE International Geoscience and Remote Sensing Symposium*, Volume 3, pp. III–210, IEEE.

Xie S, Dixon T, Holland D, Voytenko D and Vaňková I (2019) Rapid iceberg calving following removal of tightly packed pro-glacial mélange. *Nature Communications* **10**(1), 1–15.